1-2017

Temperature of the Plasmasphere from Van Allen Probes HOPE

Kevin J. Genestreti

Jerry Goldstein

Grace D. Corley
Trinity University, gcorley@trinity.edu

William Farner
Trinity University, wfarner@trinity.edu

Lynn M. Kistler

See next page for additional authors

Repository Citation

Genestreti, K.J., Goldstein, J., Corley, G.D., Farner, W., Kistler, L.M., Larsen, B.A., Mouikis, C.G., ... & Turner, N.E. (2017). Temperature of the plasmasphere from Van Allen probes HOPE. *Journal of Geophysical Research: Space Physics, 122*(1), 310-323. doi: 10.1002/2016JA023047

AGU PUBLICATIONS

JGR

Journal of Geophysical Research: Space Physics

RESEARCH ARTICLE

10.1002/2016JA023047

Temperature of the plasmasphere from Van Allen Probes HOPE

K. J. Genestreti[1,2,3], J. Goldstein[1,2], G. D. Corley[4], W. Farner[4], L. M. Kistler[5], B. A. Larsen[6], C. G. Mouikis[5], C. Ramnarace[4], R. M. Skoug[6], and N. E. Turner[4]

[1]Department of Physics and Astronomy, University of Texas at San Antonio, San Antonio, Texas, USA, [2]Space Science and Engineering Division, Southwest Research Institute, San Antonio, Texas, USA, [3]Now at Space Research Institute, Austrian Academy of Sciences, Graz, Austria, [4]Department of Physics and Astronomy, Trinity University, San Antonio, Texas, USA, [5]Space Science Center, University of New Hampshire, Durham, New Hampshire, USA, [6]Los Alamos National Laboratory, Los Alamos, New Mexico, USA

Key Points:
- Two new methods are developed to determine the temperature of cold plasmas from ESA-based data
- New methods are applied to RBSP-HOPE observations of the plasmasphere
- Scaling between plasmasphere temperature and ring current density may indicate heating in overlap region

Correspondence to:
K. J. Genestreti,
keving1098@gmail.com

Citation:
Genestreti, K. J., J. Goldstein, G. D. Corley, W. Farner, L. M. Kistler, B. A. Larsen, C. G. Mouikis, C. Ramnarace, R. M. Skoug, and N. E. Turner (2017), Temperature of the plasmasphere from Van Allen Probes HOPE, *J. Geophys. Res. Space Physics*, *122*, 310–323, doi:10.1002/2016JA023047.

Received 9 JUN 2016
Accepted 19 DEC 2016
Accepted article online 22 DEC 2016
Published online 19 JAN 2017

Abstract We introduce two novel techniques for estimating temperatures of very low energy space plasmas using, primarily, in situ data from an electrostatic analyzer mounted on a charged and moving spacecraft. The techniques are used to estimate proton temperatures during intervals where the bulk of the ion plasma is well below the energy bandpass of the analyzer. Both techniques assume that the plasma may be described by a one-dimensional $\vec{E} \times \vec{B}$ drifting Maxwellian and that the potential field and motion of the spacecraft may be accounted for in the simplest possible manner, i.e., by a linear shift of coordinates. The first technique involves the application of a constrained theoretical fit to a measured distribution function. The second technique involves the comparison of total and partial-energy number densities. Both techniques are applied to Van Allen Probes Helium, Oxygen, Proton, and Electron (HOPE) observations of the proton component of the plasmasphere during two orbits on 15 January 2013. We find that the temperatures calculated from these two order-of-magnitude-type techniques are in good agreement with typical ranges of the plasmaspheric temperature calculated using retarding potential analyzer-based measurements—generally between 0.2 and 2 eV (2000–20,000 K). We also find that the temperature is correlated with *L* shell and hot plasma density and is negatively correlated with the cold plasma density. We posit that the latter of these three relationships may be indicative of collisional or wave-driven heating of the plasmasphere in the ring current overlap region. We note that these techniques may be easily applied to similar data sets or used for a variety of purposes.

1. Introduction

The plasmasphere is cold, dense, and similar in composition to the ionosphere (mainly H+, He+, O+, and *e*–), and its motion is largely governed by $\vec{E} \times \vec{B}$ drift [*Lemaire and Gringauz*, 1998]. Many of the larger-scale dynamics of the plasmasphere (e.g., erosion, plume formation, and plume wrapping) can be described by some initially considered plasmasphere acted upon by a variable convective electric field [*Goldstein and Sandel*, 2005]. An understanding of the smaller-scale dynamics of the plasmasphere (e.g., shoulder formation and plume bifurcation) requires the consideration of coupling between inner magnetospheric electric fields and the ionosphere [*Goldstein et al.*, 2003, 2005; *Burch et al.*, 2004]. The development of further substructure (e.g., anomalous heating/cooling, wave generation/dispersion, and localized plasma sources/losses) remains an active field of research, particularly when cross-energy/cross-population interactions govern local dynamics [*Gallagher and Comfort*, 2016].

In comparison with the density, thermal structures in the plasmasphere have received little attention. Our current understanding of temperature structures in the plasmasphere is largely derived from measurements by Retarding Potential Analyzers (RPAs) on board polar-orbiting spacecraft (e.g., Dynamics Explorer, INTERBALL, and Polar) [*Kotova*, 2007; *Chappell et al.*, 2008]. Such studies have shown that the temperature of the plasmasphere is highly variable, as it depends on *L*, MLT, geomagnetic activity, solar cycle, local density, coupling with the upper ionosphere/thermosphere, and, most likely, the degree to which the plasmasphere overlaps other inner magnetospheric plasmas [*Comfort*, 1986; *Khazanov et al.*, 1996; *Gurgiolo et al.*, 2005; *Kotova*, 2007; *Gallagher and Comfort*, 2016]. RPA-based studies have increased our knowledge of the subglobal dynamics of the plasmasphere, though they are typically limited by the latitude-altitude restrictions of the polar orbit of the given spacecraft. Studies of equatorial thermal structures should be able to examine, in situ, high-altitude

and low-latitude heating processes that have been used to explain discrepancies between modeled temperatures and high-latitude observations. Such heating processes may be critically important for our understanding of the role of the plasmasphere in global magnetospheric dynamics [*Gallagher and Comfort*, 2016]. For example, heating of the dayside plasmasphere during the sunward surge/plume formation stages of convection may significantly alter the properties of the plasmaspheric ions as they convect toward the dayside magnetopause and reconnection site.

NASA's Van Allen Probes, formerly the Radiation Belt Storm Probes, launched in 2012 [*Mauk et al.*, 2013]. The two probes are in a prograde, roughly equatorial orbit with an inclination of ~10°, a period of ~9 h, and a perigee and apogee of $0.1 \times 5.8 R_E$. The Helium, Oxygen, Proton, and Electron (HOPE) instrument [*Funsten et al.*, 2013], part of the Energetic particle, Composition, and Thermal plasma (ECT) instrument suite [*Spence et al.*, 2013], consists of coupled electrostatic and time-of-flight analyzers. HOPE measures fluxes for its four singly charged namesake particle species over a nominal energy range of 1 – 50,000 eV for five polar angles and 16 elevation (spin) angles. Full 3-D flux measurements are obtained at approximately the spacecraft spin rate (spin rate of ~1/11 Hz and HOPE sample rate of ~1/12 Hz), where ion and electron fluxes are measured on alternate spins. Spacecraft potential measurements are provided by the Electric Field and Waves (EFW) instrument [*Wygant et al.*, 2013]. Studies of the charging of Van Allen Probes in the plasmasphere have showed that the spacecraft potential can exceed the low-energy threshold of HOPE (1 eV) or upward of 100% of the nominal low-energy threshold of HOPE [*Goldstein et al.*, 2014; *Sarno-Smith et al.*, 2015, 2016]. Even nominally, the low-energy threshold of HOPE is greater than the bulk kinetic and thermal energies of the plasmasphere. The observable portion of the ion distribution may increase when the ram velocity of the spacecraft ($\vec{V}_{SC}$) and the bulk velocity of the plasmasphere ($\vec{u}$) are such that $\left|\vec{V}_{SC} - \vec{u}\right| \geq \left|\vec{u}\right|$, though the partial-energy ion density observed by HOPE can be less than a tenth of the total energy number density of the plasmasphere [*Goldstein et al.*, 2014].

In this study, we calculate the scalar temperature of the low-energy ($\lesssim$ 10 eV) proton component of the plasmasphere using data from Van Allen Probes HOPE and EFW. In the next section we provide an overview of the data products used in this study. In section 3 we describe two techniques for calculating the temperatures of low-energy protons. The first technique involves the application of a theoretical fit to the fraction of the distribution function observed by HOPE. The second technique involves the comparison of the partial-energy number density, calculated over the energy range of HOPE (see Appendix A), with the total energy number density, calculated using the waves or spacecraft potential data. In section 4 we apply these techniques to HOPE data during multiple plasmasphere intervals on 15 January 2013. In section 5 we summarize our results and discuss the means by which these rough techniques may be improved upon in the future.

2. Data Products and Preparation

HOPE omnidirectional fluxes are used throughout this paper. These data files were from the third release (labeled rel03) of the level 3 (L3) pitch angle-resolved fluxes and were obtained from the ECT data repository (http://www.rbsp-ect.lanl.gov) on 12 April 2016. These specific versions and dates may be important as, in the future, these data may be subject to retroactive calibration.

We differentiate between the energies reported by HOPE and the initial energies of the ambient plasma, prior to perturbation by the charged and moving spacecraft. The reported and ambient particle energies differ most significantly near the low-energy threshold of HOPE, where (a) the ram energy of the spacecraft; (b) the electric potential of the spacecraft, a consequence of photoionization; and (c) electric potential within the surrounding plasma, a consequence of charge separation in the spacecraft wake may be comparable to the bulk kinetic and thermal energies of the plasma. Approximately, the effect of (a) is to alter the "effective" bulk velocity of the plasma in the rest frame of the spacecraft. The approximate effect of (b) is to add an offset between the reported energies and the initial energy of the plasma being measured. The effect of (b) is accounted for first, as the conversion from flux to phase space density (PSD) requires knowledge of the energy of the plasma. As in previous studies [*Comfort et al.*, 1985], we assume that the structure of the spacecraft potential field is negligible, such that the reported energies ($\mathcal{E}$) may be adjusted according to $\mathcal{E}' = \mathcal{E} + q\Phi_{SC}$, where the spacecraft potential (Φ_{SC}) is obtained from EFW data. The effect of (a) is accounted for during the calculation of the effective bulk velocity of the plasma, as is discussed in the following section. We do not account for the effects of (c).

Other RBSP data used in this study include (a) spacecraft ephemeris, (b) densities derived from the waves data, (c) the spacecraft potential and potential-derived densities, and (d) the spin resolution magnetic field strength. The spacecraft ephemeris was obtained from the HOPE data files. The waves-derived densities were taken from *Goldstein et al.* [2014], which also described the method for analyzing the waves data and determining subsequent densities. Spacecraft potential and potential-derived density data were obtained from the EFW data repository (http://www.space.umn.edu/rbspefw-data). Magnetic field data were obtained from the Electric and Magnetic Field Instrument Suite and Integrated Science (EMFISIS) data repository (http://emfisis.physics.uiowa.edu/).

3. Techniques for Estimating Temperatures

3.1. Overview and Common Assumptions

In this paper, we discuss two novel techniques for calculating the temperatures of very low energy plasmas ($\lesssim 1$ eV) from in situ data taken from an electrostatic analyzer mounted on a charged and moving spacecraft. The techniques are useful when the bulk of the plasma is below the effective energy range of the instrument; otherwise, a number of other assumptions may be used to enable more direct or simplified calculations of the temperature by fitting or numerical integration [cf. *Comfort*, 1986]. These two techniques may be easily generalized to similar instruments and various plasma particle species, though the focus of this study is HOPE observations of the proton component of the plasmasphere.

These two (not entirely dissimilar) methods for calculating temperatures share a number of assumptions. First, as discussed in the previous section, we assume that the relationship between the ambient ($\mathcal{E}'$) and measured ($\mathcal{E}$) plasma energies are related by $\mathcal{E}' = \mathcal{E} + q\Phi_{SC}$ in the frame of the moving spacecraft.

Next, we assume that the bulk velocity of the plasma in the spacecraft frame, $\vec{u}$, is equivalent to the difference of the $\vec{E}\times\vec{B}$ drift and the spacecraft velocities, i.e., $\vec{u} = \vec{u}_{E\times B} - \vec{V}_{SC}$. The magnetic field, $\vec{B}$, is determined in situ by the EMFISIS magnetometer. The electric field, $\vec{E}$, is taken to be the sum of the corotation and convection electric fields. Corotation is assumed to occur at exactly the rotation rate of the planet; i.e., we do not account for subcorotation. The convective electric field is approximated by a Volland-Stern potential [*Volland*, 1973; *Stern*, 1975] model, which is parameterized by the solar wind electric field and a shielding factor of 2 [*Goldstein and Sandel*, 2005; *Goldstein et al.*, 2014]. Errors in the modeled magnetospheric electric field enter into the temperature estimation methods (outlined in the following two sections) in a complex manner. Generally, errors in $\vec{u}_{E\times B}$ are inconsequential at small L, where $\vec{u}$ is dominated by $\vec{V}_{SC}$. At large L, errors in the modeled electric field might add considerable errors in the temperature depending on (a) the method used to determine the temperature, (b) the difference between the bulk kinetic, thermal, and smallest observable energies, and (c) the strength of the convective electric field. For our case study, we found that large ($\pm$200%) purposefully added errors in E_{conv} can alter the fit-determined and partial-energy number density (PEND)-determined temperatures by $\sim$10% and $\sim$1% (respectively) at $L \geq 4$. We also found small differences in the temperature (less than 1% at $L < 4$ and $\sim$6% at $L \geq 4$) when in situ measurements or the Earth-centered tilt-free dipole model were used to calculate the magnetic field, despite the fact that a large ($\sim$25%) mean deviation from the tilt-free dipole model was observed. (For a more detailed discussion on these errors, see Appendix B).

The velocity of the spacecraft is calculated by first-order differentiation of the spacecraft ephemeris. Note that this method of calculating $\vec{u}$ neglects the fact that the low-energy threshold of HOPE may vary with the instrument look direction; the lowest possible "detectable" energy may vary by less than a tenth of an eV if the aperture of HOPE is aligned or antialigned with the spacecraft velocity.

Isotropy is also assumed, such that the distribution of the plasma can be studied one-dimensionally. (Note that while the assumption of isotropy has been used in past studies [cf. *Comfort et al.*, 1985], anisotropic distributions have also been reported in the plasmasphere [*Fuselier and Anderson*, 1996]). This assumption is not required by but is useful for the simplification of the fit-based technique for calculating temperatures (discussed in the following section). The assumption of isotropy is required by the partial-energy number density (PEND) technique, as is discussed in section 3.3. Following from this assumption of isotropy, all temperatures calculated in this paper represent a scalar approximation of the possibly differing, directional temperatures. Note that if the plasma is anisotropic, then the scalar temperatures that can be calculated with these techniques should still be $T = \left(T_{\parallel} + 2T_{\perp}\right)/3$. Thus, while this is not an accurate description of either the parallel or perpendicular temperatures of an anisotropic plasma, these techniques may still be useful for identifying absolute heating/cooling.

Finally, we assume that the plasma can be well-represented by a (drifting and 1-D) Maxwellian-type Gaussian distribution. As the bulk (≥ 90%) of the plasmaspheric ions are below the measurable threshold of HOPE, this or some similar assumption is required, such that the observations of HOPE may be extrapolated to lower energies. Previous measurements reported from Dynamics Explorer retarding ion mass spectrometer (DE-RIMS) show that the very low energy component of the plasmasphere (≲10 eV) is generally well-represented by a Maxwellian [*Comfort et al.*, 1985; *Comfort*, 1996]. A kappa-like tail may also be present at higher energies than the Maxwellian-like bulk of the distribution. Since it is not easily separated from the ring current, which may overlap the plasmasphere, the focus of this investigation is the low-energy (≲10 eV) portion of the distribution.

Appendix B provides an examination of the theoretical and practical errors associated with this fit-based technique.

3.2. Fit-Based Method for Estimating *T*

The first method for calculating temperatures involves a least squares fit of the HOPE-measured omnidirectional phase space densities with a 1-D drifting Maxwellian of the form

$$f_p(v) = n_p \left(\frac{m_p}{2\pi k T_p}\right)^{\frac{3}{2}} \exp\left[-\frac{m\left(v-u_{\text{eff}}\right)^2}{2kT_p}\right], \tag{1}$$

where f_p is the proton phase space density, n_p is the total energy number density of protons, T_p is the scalar proton temperature, v is the velocity coordinate, and u_{eff} is the effective bulk velocity, i.e., the $\vec{E}\times\vec{B}$ velocity in the moving frame of the spacecraft. We convert HOPE-measured omnidirectional proton differential number fluxes, or $J_p(\mathcal{E}')$, to proton phase space densities, $f_p(\mathcal{E}')$, with the relation

$$f_p(\mathcal{E}') = J_p(\mathcal{E}')\frac{m_p}{2\mathcal{E}'}. \tag{2}$$

The measured values of $f_p(\mathcal{E}')$ are weighted by their uncertainty, which is taken to be Poisson counting uncertainty, e.g., $f_p(\mathcal{E}') = f_p(\mathcal{E}') \pm \epsilon(\mathcal{E}')80\sqrt{C_p(\mathcal{E}')/80}$, where $C_p(\mathcal{E}')$ is the angle-integrated proton counts per energy, $\epsilon(\mathcal{E}')$ is an energy-dependent factor of proportionality related to the geometric factor of the instrument, and 80 is the total number of angular bins (5 × 16). To determine $\epsilon(\mathcal{E}')$, we simply use $\epsilon(\mathcal{E}') \equiv f_p(\mathcal{E}')/C_p(\mathcal{E}')$, which is directly calculated from the counts and flux data provided in the HOPE data files. (Note that a more rigorous definition of ϵ should account for nonuniformities in the distribution of counts per look direction.)

The fit is applied to all data points within $\mathcal{E}' \leq 3\mathcal{E}_{\text{bulk}}$ (using the properties of a Gaussian, only ~0.3% of the plasmasphere number density should be above $\mathcal{E}' \geq 3\mathcal{E}_{\text{bulk}}$ for $\mathcal{E}_{\text{bulk}} \approx \mathcal{E}_{\text{therm}}$, where $\mathcal{E}_{\text{therm}}$ and $\mathcal{E}_{\text{bulk}}$ are the thermal and drift kinetic energies, respectively). We exclude instances where fewer than three data points are available in this energy range, as the residual error should be 0 when the number of data points matches the number of open parameters. Solutions are degenerate when there are fewer data points than the number of open parameters.

The total energy proton number density, n_p, is not constrained prior to the fit, despite the fact that n_p is likely very similar in value to the total number densities from EFW and EMFISIS over the majority of the plasmasphere interval examined in this study. We do not constrain n_p because (a) the composition of the plasmasphere may vary, and constraining n_p might negatively affect the general application of this technique, (b) it is not possible to calculate the composition over all energies from HOPE data alone, so it is difficult to accurately account for the error in any assumption on the composition of the plasmasphere, and (c) if n_p is not constrained, then it is possible to compare its fit-determined value to the total number densities from EFW/EMFISIS as a rough check for the quality of a given fit.

3.3. PEND Method for Estimating *T*

Another technique for determining temperatures is what we are calling the partial-energy number density, or PEND, technique. This technique requires (a) a measure of the total number density, (b) a measure of the partial-energy number density (see Appendix A), and (c) an estimate for the bulk kinetic energy. As with the fit technique, the PEND technique assumes that the plasma can be described by a drifting isotropic Maxwellian.

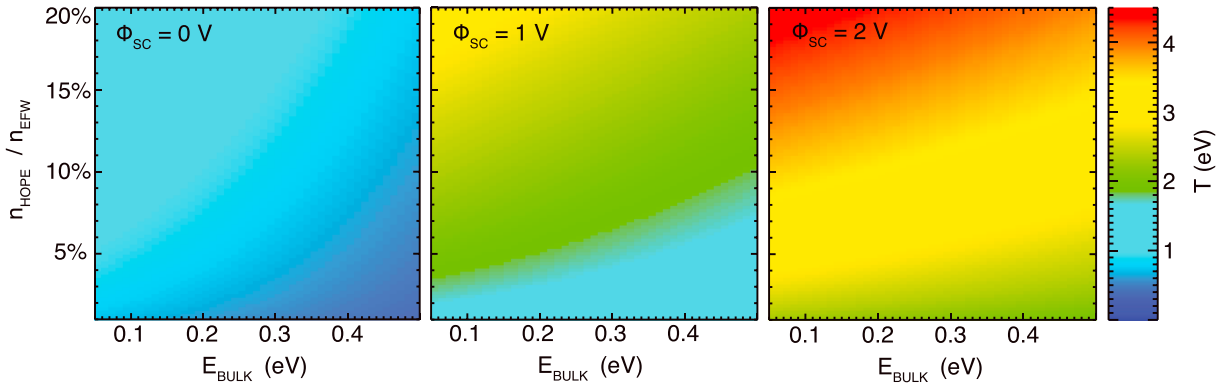

Figure 1. A graphical representation of equation (5). Values of Φ_{SC} and ranges of all axes (except temperature, which is the dependent variable) have been selected as representative of their values during the plasmasphere intervals of the 15 January 2013 event, which are shown in Figure 2.

If these assumptions are realistic, then the fraction of the plasma number density that appears in the energy window of HOPE should be

$$\frac{n\left(\mathcal{E} \geq \mathcal{E}'_{\mathrm{HOPE,min}}\right)}{n(\mathcal{E} \geq 0)} = 1 - \mathrm{erf}\left(\frac{j}{\sqrt{2}}\right), \tag{3}$$

where $n(\mathcal{E} \geq 0)$ is the total number density obtained from either the spacecraft potential or upper hybrid frequency, $n\left(\mathcal{E} \geq \mathcal{E}'_{\mathrm{HOPE,min}}\right)$ is the partial-energy number density obtained from direct numerical integration of HOPE fluxes, and j is the number of Gaussian standard deviations (commonly denoted as σ) between the bulk kinetic energy and the low-energy threshold of HOPE. For a 1-D Maxwellian-type Gaussian with a thermal energy equal to $T_E = kT/2$, the standard deviation is twice the temperature, so

$$2jT \equiv \left(\mathcal{E}'_{\mathrm{HOPE,min}} - \mathcal{E}_{\mathrm{bulk}}\right), \tag{4}$$

which can be used along with equation (3) to solve for temperature in terms of measurable quantities, as written in equation (5).

$$T = \frac{\sqrt{2}\left(\mathcal{E}'_{\mathrm{HOPE,min}} - \mathcal{E}_{\mathrm{bulk}}\right)}{\mathrm{erf}^{-1}\left[1 - \frac{n(\mathcal{E} \geq \mathcal{E}'_{\mathrm{HOPE,min}})}{n(\mathcal{E} \geq 0)}\right]}. \tag{5}$$

Figure 1 provides a graphical representation of the coupling between the temperature, density ratio, bulk energy, and spacecraft potential in equation (5). Generally, Figure 1 shows that when the temperature is large, a larger portion of the distribution function is located within the energy range of HOPE.

For all instances in this study where the PEND technique has been applied, we have calculated the partial-energy number density over the range $\mathcal{E}'_{\mathrm{HOPE,min}} \leq \mathcal{E} \leq 20$ eV (rather than the energy range $\mathcal{E} \geq \mathcal{E}'_{\mathrm{HOPE,min}}$). This is done to exclude fluxes at higher ring current-like energies, which we do not consider as an extension of the cold (assumed Maxwellian-like) plasmaspheric population (i.e., the PEND temperature does not change significantly if 10 eV $\leq \mathcal{E}' \leq$ 10 keV is chosen as the high-energy cutoff). Note that the exact value of this upper bound does not affect the resulting values of the temperature significantly, as particle fluxes at ring current-like energies are generally insignificant compared to fluxes at plasmasphere-like energies. This is in contrast to the fit method, which uses a more dynamic value of $3\mathcal{E}_{\mathrm{bulk}}$ as the high-energy cutoff for the data used in the temperature calculation. Unlike the fit method, which is sensitive to non-Maxwellian-like data points, the PEND method is not affected by non-Maxwellian-like data, so long as the density of the non-Maxwellian-like plasma is very small.

The advantages of the PEND technique are that (a) it can be applied much more easily than the fit-based technique and (b) it is expected to be less error-prone than the fitting technique when the bulk kinetic and thermal energies of the plasma are well below the effective low-energy threshold of HOPE

$\left(\mathcal{E}_{bulk} + \mathcal{E}_{therm} \ll \mathcal{E}'_{HOPE,min}\right)$. The uncertainties in the PEND technique are a function of the error in the bulk velocity estimation and as the Poisson uncertainty in the count rates and the truncation error for the first-order integration scheme used to calculate the partial-energy number density (see Appendix A). Error in the modeled bulk velocity, which is difficult to account for exactly and explicitly, should have only a minimal impact on the PEND-determined temperature, as the bulk energy (tenths of an eV) is generally much less than the low-energy threshold of HOPE (upward of 1 eV).

One of the disadvantages of the PEND technique is that it requires some assumption regarding the composition of the plasma, as the total number density from either EFW or EMFISIS is being compared to partial-species number densities from HOPE. In this study, we have applied the PEND technique assuming that the ion plasma is composed entirely of protons. If the composition was reasonably well-constrained, it may be possible to also use this technique to estimate temperatures for minor ion species, though we have not done so in this study. Another disadvantage is that the PEND technique does not provide any information regarding how "Maxwellian like" the plasma actually is, whereas numerical analysis can be used to extract error estimates for the fit-based technique. Another disadvantage of the PEND technique is that, as compared to the fit-based technique, there is little room for improvement. A fundamental aspect of the PEND technique is that the total density (a directionless measurement) is compared to fluxes from HOPE (a directional measurement), and as such, any information regarding anisotropy is lost. While the fit-based technique may be developed in the future to obtain parallel and perpendicular temperatures separately, the PEND technique is inherently a method for calculating scalar temperatures.

4. Event Study

4.1. Event Overview

We analyze data from Van Allen Probes A over the course of two orbits (~18 total hours) on 15 January 2013, starting at 02:00 UT. During this interval, the solar wind velocity decreased from an initial value of ~500 km/s to ~425 km/s and the IMF B_Z oscillated aperiodically within ±4 nT. Geomagnetic activity was negligible, with a minimum *Dst* of −26 nT and a maximum *Kp* of 2. The variable inner magnetospheric electric field, which is taken to be 0.15 times the solar wind electric field for $B_Z \leq 0$ and 0 for $B_Z \geq 0$ [*Goldstein et al.*, 2014], reached a maximum value of 0.25 mV/m. Significantly stronger convection was observed 2 days later, on 17–18 January 2013.

An overview of the 15 January 2013 event is shown in Figure 2. Van Allen Probes A (henceforth referred to as RBSP-A) was initially located in the duskside inner plasmasphere at $L = 1.8$ and MLT = 20, having just exited the inner radiation belt, outbound from perigee. RBSP-A exited the plasmasphere at ~04:00, as judged by the decrease in low-energy proton flux observed by HOPE (Figure 2a) and the sharp decrease in the total number densities extracted from the waves data and obtained from the spacecraft potential (Figure 2d). The entries and exits to and from the plasmasphere are also accompanied by sharp increases and decreases (respectively) in the spacecraft potential (Figure 2h). The plasmasphere intervals in Figure 2 were defined by the total energy electron number density, $n_e > 20$ cm^{-3} [*Goldstein et al.*, 2014]. RBSP-A reached apogee at ~06:00 UT, L=6, and MLT = 2.5. The probe reentered the plasmasphere on the dawnside at 08:20 UT, $L = 5$, and MLT = 5.2. Low-energy measurements from HOPE were no longer available after RBSP-A reentered the inner radiation at 10:20 UT, inbound toward perigee. For 40min following 10:20 UT, RBSP-HOPE entered its perigee mode, where energies below ~23 eV are not measured. The parameters for the second orbit were similar to those of the first orbit. For the second orbit, RBSP-A exited the plasmasphere in the outbound direction at 12:35 UT and reentered the plasmasphere in the inbound direction at 17:45 UT. The equatorial location of the spacecraft during these two orbits is shown in Figure 2j.

During the first two (outbound and inbound) plasmasphere intervals, the spacecraft potential (Figure 2g) was $0 \leq \Phi_{SC} \leq 2$ V, which corresponds to 0% and 200% of the nominal low-energy threshold of HOPE, respectively. The effective bulk speed ($|\vec{u}'|$), or the magnitude of the difference of the modeled $\vec{E} \times \vec{B}$ drift and spacecraft velocities $\left(|\vec{u}'| = |\vec{u}_{EB} - \vec{V}_{SC}|\right)$, varied between 8 and 4 km/s. For protons, this corresponds to bulk kinetic energies of 0.3 and 0.08 eV, respectively. For a Maxwellian proton distribution with a temperature and bulk energy of 1/3 eV, approximately 5% of the distribution should be within the energy threshold of HOPE for $\Phi_{SC} = 0$. This is roughly consistent with the ratio of the total (derived from EFW and EMFISIS) and partial-energy (calculated directly from HOPE; see Appendix A) densities shown in Figure 2e.

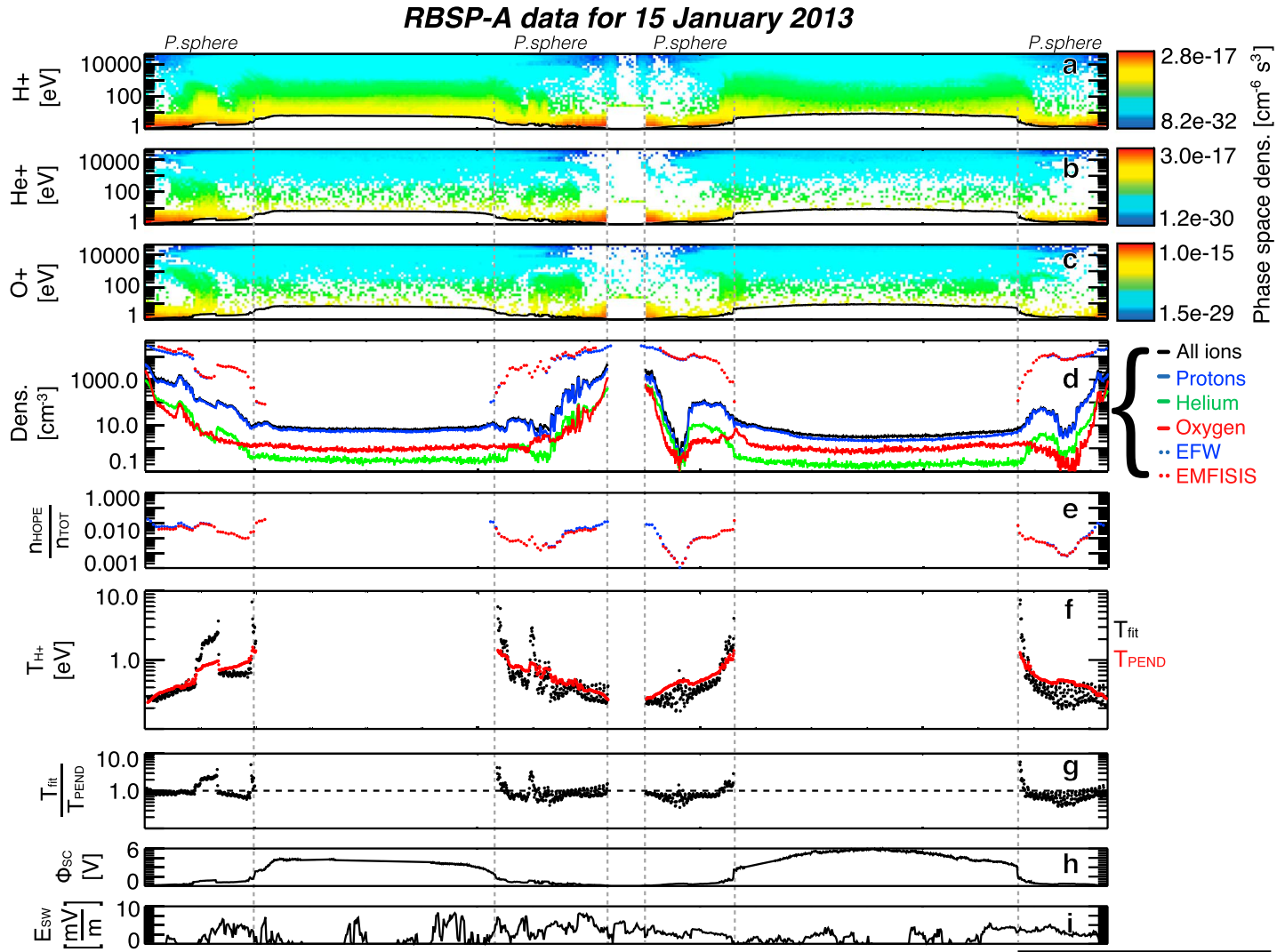

Figure 2. Overview of RBSP-A and solar wind data for two orbits of RBSP on 15 January 2013. Vertical grey dashed lines delimit plasmasphere intervals from ring current and radiation belt intervals. Omnidirectional energy intensity-time spectrograms for (a) protons, (b) helium, and (c) oxygen. The reported energy values have been shifted according to $\mathcal{E}' = \mathcal{E} + \Phi_{SC}$, and the solid black line is the effective low-energy threshold $\left(\mathcal{E}'_{HOPE,min} = \mathcal{E}_{HOPE,min} + \Phi_{SC}\right)$. (d) Number densities calculated from HOPE over its full energy range (see Appendix A) and total densities extracted from the waves data (labeled EMFISIS) and the spacecraft potential (labeled EFW). (e) The fraction of the total plasma number density that appears within the energy range of HOPE (red: n_{HOPE}/n_{EFW}, blue: $n_{HOPE}/n_{EMFISIS}$). (f) The temperature of cold plasmaspheric protons, calculated with the fit-based (black) and PEND (red) techniques. (g) The ratio of the temperatures from the two techniques. (h) Spacecraft potential from EFW. (i) The solar wind electric field, positive for southward IMF B_Z and zero otherwise. (j) The position of RBSP-A in the X-Y_{SM} plane for the first (red) and second (blue) orbits, where the initial position, final position, and position at 10:30 UT are labeled with an asterisk, a diamond, and a plus sign, respectively.

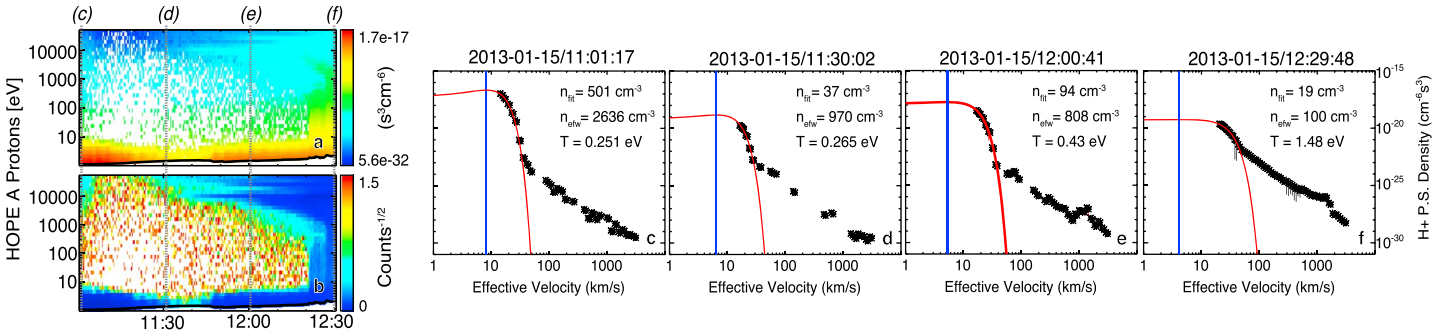

Figure 3. (a) Energy-time spectrogram. (b) Fractional uncertainty ($\sqrt{\text{Counts}}/\text{Counts}$). Shown in black in Figures 3a and 3b is the effective low-energy threshold of HOPE (1 eV + Φ_{SC}). (c–f) Example Maxwellian fits (red) to spacecraft potential-adjusted HOPE flux data (black), which are determined using the modeled effective bulk velocity (blue). Uncertainties in the HOPE fluxes (black vertical lines) are generally not visible, as they are generally smaller than the symbols (asterisks) used to denote fluxes, which appear large given the large ranges of the *Y* axes. Figure 3c is an example of a "good quality" fit, where a large amount of the low-temperature plasmasphere appears above $\mathcal{E} \geq \mathcal{E}_{\text{min,HOPE}}$ due to the large spacecraft velocity. Figure 3b is a medium-quality fit, where the bulk velocity and the temperature are both small. Figure 3c is a good quality fit, where the spacecraft velocity is small but the plasma is warm. Figure 3d is a poor quality fit, where the plasmasphere is hot but the spacecraft potential is large, the spacecraft velocity is small, and there is significant overlap between the ring current and the plasmasphere.

4.2. Summary of Deduced Temperatures

The temperature of the low-energy ($\mathcal{E} \lesssim 10$ eV) component of the protons is shown in Figure 2f. The temperature is calculated when HOPE is in its nominal mode of operation and the total number density, derived from the spacecraft potential and/or upper hybrid frequency (labeled n_{EFW} and n_{EMFISIS} in Figure 2d), exceeds 20 cm^{-3}. The methods used to calculate the temperature are described in detail in section 3.

The ratio of the two temperatures, which are calculated with the fit-based and PEND techniques, is shown in Figure 2g. There is an average 32% difference between the temperatures from the fit-based and PEND techniques. The best agreement between these two methods occurs when there is little overlap between plasmas with ring current-like and plasmasphere-like energies. When there is a significant amount of overlap between these two populations, the fit-based method generally predicts a higher temperature than the PEND method. As fluxes of the higher-energy ring current plasmas are significantly lower than the fluxes in the lower energy range of the plasmasphere, the overlap between the two populations has less of an impact on lower-order moments (e.g., density) than higher-order moments (e.g., temperature). An example of a poor fit, determined for an interval with considerable overlap between low-energy and ring current energy protons, is shown in Figure 3f. Examples of good and intermediate quality fits are shown in Figures 3c–3e.

Semiperiodic oscillations are visible in the fit-based temperature (Figure 2f) and the low-energy portion of the energy intensity-time spectrograms (Figures 2a–2c), which occur with a period of roughly 260 s, or ~22 spin periods. Similar oscillations are also seen in the partial-energy number density (Figure 2d) and in T_{PEND},

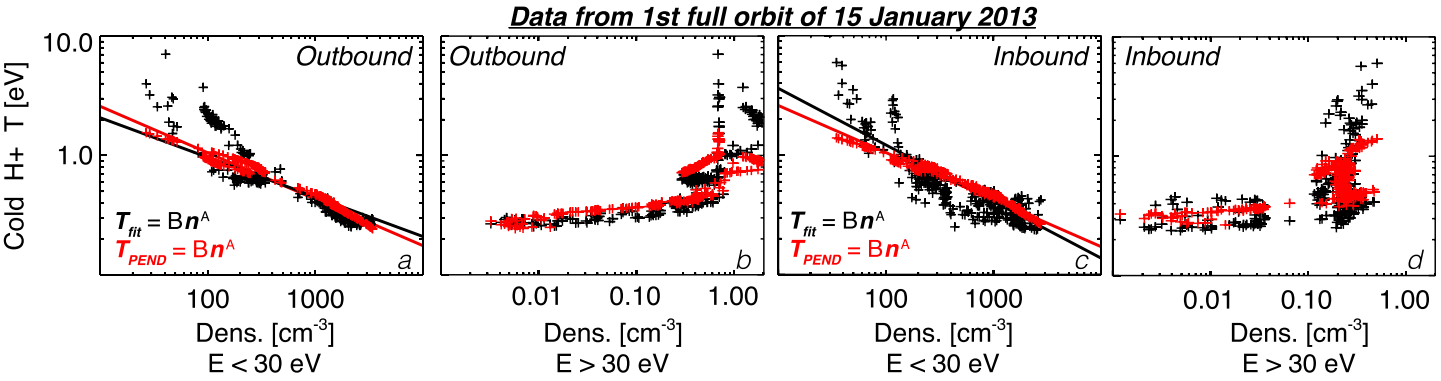

Figure 4. Temperatures of the low-energy protons as a function of (a and c) low-energy plasma density and (b and d) ring current density for the outbound pass through the duskside plasmasphere (Figures 4a and 4b) and inbound pass through the dawnside plasmasphere (Figures 4c and 4d). Black and red colors indicate the method used to calculate the temperature and correspond to the fit-based and PEND methods, respectively. Black and red solid lines are fits of the form $T = Bn^A$; *A* and *B* are listed in Table 1.

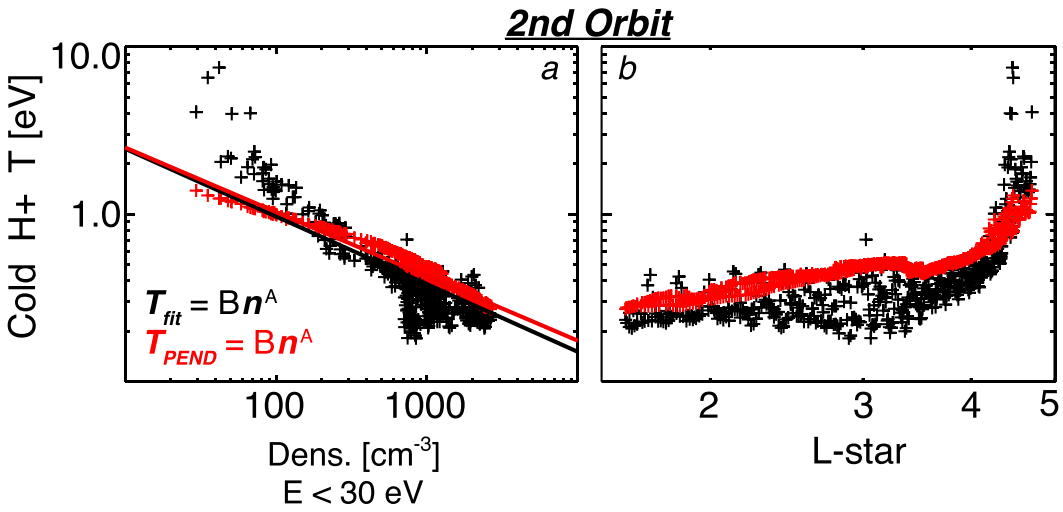

Figure 5. Plasma parameters for the second full orbit of 15 January 2013. (a) Temperature of the cold protons versus total number density of low-energy (≤ 30 eV) plasma with linear fits of the form $T = Bn^A$ (A and B are listed in Table 1). (b) Temperature versus L. Black (red) data are for temperatures calculated using the fit-based (PEND) technique.

though with significantly smaller amplitudes that are not apparent in this plot range. These are assumed to be an artifact of the instrument rather than a physical property of the plasma. The rate at which HOPE sweeps through energy direction space is slightly out of sync with the spacecraft spin rate, which leads to an oversampling of a portion of energy-solid angle space. The peaks and (troughs) of these oscillations likely correspond to instances where the oversampled portion of the solid angle is antialigned (aligned) with the bulk velocity of the plasma in the spacecraft rest frame. These oscillations are most pronounced when the temperature and bulk energies are low, which is consistent with the theory that they result from a harmonic between the directions of the oversampled phase space and the effective bulk velocity. Thus, these oscillations should not appear if the effects of oversampling were carefully removed, which is not done in this study.

Previous studies have shown that typically, the temperature of the ion component of the plasmasphere is in the range 2000–20,000K, or 0.2–2 eV [*Kotova*, 2007]. As mentioned in section 1, many of these studies have used 1990s era data from RPAs mounted on low-altitude high-latitude orbiting observatories. As shown in Figure 2f, our two methods for estimating order-of-magnitude scalar temperatures from RBSP-HOPE data predict a temperature range of roughly 0.2–2 eV, with the fit-based method predicting larger temperatures than the PEND method in regions where the bulk of the plasmaspheric ions are below the effective energy range of HOPE. There are also steep gradients in the proton temperature that are observed during similarly steep gradients in the total plasma number density (red and blue dotted lines in Figure 2d), a feature that has previously been observed in high-latitude DE-RIMS data [*Comfort*, 1986].

4.3. Coupling Between Plasma Parameters

In Figure 4, the cold proton temperature is shown as a function of the densities of cold and warm plasma. Here we only show data from the first full orbit of 15 January 2013. As shown in Figure 4, the cold ion density and the temperature are anticorrelated. Similar trends have been identified implicitly in a number of studies, where the temperature and density are negatively (positively) correlated with L [cf. *Comfort*, 1986]. We have quantified this relationship by fitting the data with functions of the form $T = Bn^A$, which are shown in Figures 4a, 4c, and 5a and listed in Table 1. The hot ion density and the temperature are positively correlated,

Table 1. Parameters and 2σ Uncertainties (95% Confidence) for Best Fit Lines of the Form $T = Bn^A$, Which Are Shown in Figures 4a, 4c, and 5a[a]

	Outbound (Figure 4a)	Inbound (Figure 4c)	Orbit 2 (Figure 5a)
A	−0.33 ± 0.095, **−0.39 ± 0.066**	−0.47 ± 0.096, **−0.39 ± 0.066**	−0.41 ± 0.014, **−0.38 ± 0.036**
B	10.37 ± 2.04, **6.34 ± 2.01**	4.51 ± 2.10, **6.25 ± 2.01**	6.24 ± 2.03, **6.01 ± 2.01**

[a]Normal lettering: fit-determined temperatures, bold lettering: PEND-determined temperatures.

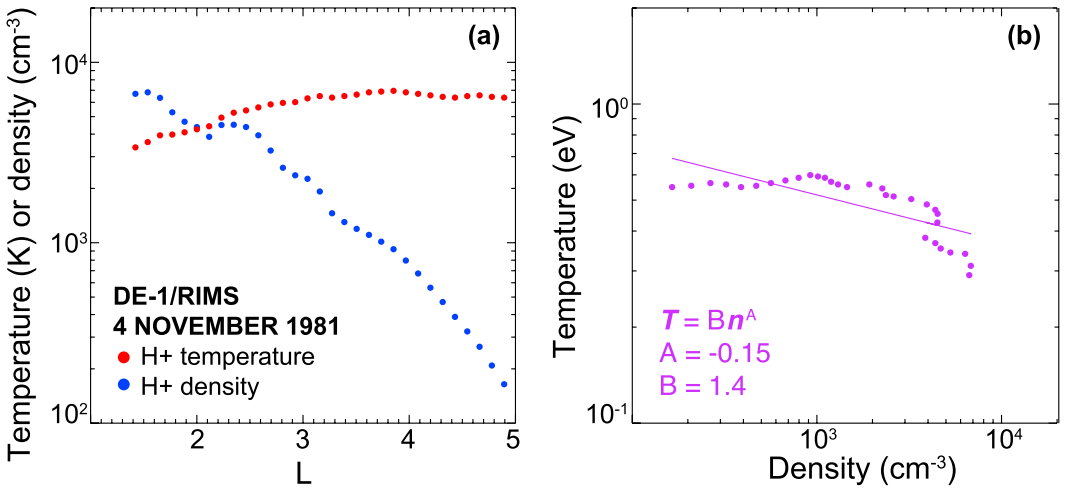

Figure 6. (a) High-latitude plasmaspheric temperatures and densities over the course of one orbit of DE-RIMS on 4 November 1981 (digitally extracted from Figure 2 of *Comfort et al.* [1988]). (b) Correlated densities and temperatures, which have been extracted digitally from *Comfort et al.* [1988] and fit with a function of the form $T = Bn^A$.

which may indicate that collisional or wave heating of the plasmasphere takes place in the ring current–plasmasphere overlap region [*Khazanov et al.*, 1996; *Gallagher and Comfort*, 2016]. The aforementioned trends are visible regardless of the method used to calculate the temperature. The previously discussed oscillations in the fit-based temperature, which appeared to be more pronounced during the inbound passes through the plasmasphere (Figure 2f), are also visible in Figures 4c and 4d.

For the second orbit (~11:00–19:20 UT), as compared to the first orbit (~02:00–08:20), there was relatively little overlap between ion fluxes with ring current-like and plasmasphere-like energies (see Figures 2a–2c). As such, it is easier to isolate the relationship between the cold ion temperature and L, which is shown in Figure 5. This positive correlation between the temperature and L has been shown in previous studies [*Comfort et al.*, 1985; *Comfort*, 1996; *Kotova et al.*, 2008] and is consistent with (a) the inverse correlation between the temperature and cold ion density and (b) the inverse relationship between the cold ion density and L.

The parameters of the fit lines, shown in Figures 4a, 4c, and 5a and listed in Table 1, can be compared to previous off-equatorial measurements of the plasmaspheric proton temperature and density from DE-RIMS data. Figure 6a shows data from Figure 2 of *Comfort et al.* [1988], which reported correlated variations in the density and temperature versus L shell during a DE-RIMS orbit on 4 November 1981 ($Kp = 1$, MLT = 19.7). The densities and temperatures were digitally extracted from the *Comfort et al.* [1988] figure, then plotted against one another and fit with a function of the form $T = Bn^A$. This is shown in Figure 6b, which also explicitly shows the inverse relationship between density and temperature discussed in the first paragraph of this section. The decay constant in the fit of Figure 6b is −0.15, which is approximately half of the average decay constant we have identified with RBSP-HOPE data. We consider the difference between this high-latitude decay rate and the equatorial decay rates listed in Table 1 to be further evidence that the ionospheric plasma, which is the source of the plasmasphere, becomes heated upon interacting with hot plasmas near the equator.

5. Conclusions and Future Work

We have introduced two new techniques for estimating the temperatures of cold ions using, primarily, data from electrostatic analyzer-based instruments. Both techniques assume that the cold plasma can be represented by an isotropic and $\vec{E} \times \vec{B}$ drifting Maxwellian. The fit-based technique involves fitting a constrained Maxwellian distribution function to energy flux spectra. The PEND technique involves comparing the partial-energy number density, calculated over a known energy range, with the total plasma number density, calculated from the upper hybrid frequency or estimated from the spacecraft potential. We have applied these techniques to obtain temperatures of the proton component of the plasmasphere from HOPE data during two orbits of RBSP on 13 January 2015. We found that both techniques yielded temperatures in the range ~0.2–2 eV, which is roughly consistent with results from previous RPA-based studies [*Kotova*, 2007].

We also found that using these techniques, we were able to reproduce many of the thermal properties of the plasmasphere that have been previously identified, including anticorrelations between the temperature and (a) the cold plasma number density and (b) L shell. We also identified a rough positive correlation between the temperature of the plasmasphere and the density of hot ring current-like ions.

Several caveats should be considered before either method for determining temperatures is implemented. First, both techniques may overestimate the temperature of the plasmasphere for cases where the relative densities of cold and hot ions are comparable, though the PEND method is significantly less susceptible to errors of this kind than the fit-based method, by virtue of the fact that PEND is inherently a method for determining a high-order moment (temperature) from a low-order moment (density). Though standard σ uncertainties are more easily obtained for temperatures obtained via the fit-based method, we note that these uncertainties are small compared to additional error sources, namely, the error resulting from the phase space oversampling caused by the difference in the spacecraft and HOPE spin phases (see discussion in section 4.1). Again, due to its low-order nature, the PEND technique is less susceptible to errors of this type than the fit-based technique. (Additional sources of error for both techniques are discussed in Appendix B).

There is significant room for development of both the fit-based and PEND techniques. For both techniques, it would be desirable to fit the higher-energy ($\mathcal{E} \geq 30$ eV) component of the plasma independently, then subtract these fit-determined fluxes from the measured fluxes at lower plasmasphere-like energies. For the previously discussed reasons, this subtraction should have a larger impact for the fit-based technique and should only be necessary when the relative densities of the two populations are comparable. It would also be desirable to expand the fit-based technique such that temperatures can be obtained from two- or three-axes directional fluxes. In doing so, it would be possible to obtain a complete temperature tensor. Differences between perpendicular and parallel temperatures may be critically important for understanding sources, losses, and the nature of the coupling between the cold and overlapping plasmas. It would be desirable to expand the fit-based and PEND methods such that they could be used to determine the temperatures of minor ion species and cold electrons. The accuracy of both methods may also be improved in the future if a more sophisticated model of the $\vec{E} \times \vec{B}$ drift were used, for example, if the shielding and sub-auroral polarization stream (SAPS) electric fields were included, if subcorotation were considered [*Burch et al.*, 2004], or if a more sophisticated model of the magnetic field was considered.

In the future, we will apply these techniques to calculate the temperature of the plasmaspheric plume using data from the Hot Plasma Composition Analyzer on board the Magnetospheric Multi-Scale mission. Other future studies may include (a) a reanalysis of this event using data from both of the Van Allen Probes, such that the temporal and spatial variations in the ring current-plasmasphere overlap region could be discriminated, and (b) an analysis of the waves data and collision frequency to determine the nature of the plasmaspheric heating.

Appendix A: Partial-Energy Number Density Calculation

As in *Goldstein et al.* [2014] and *Sarno-Smith et al.* [2015], we use the discrete Riemannian sum

$$n_s \cong 4\pi\sqrt{\frac{m_s}{2}}\sum_i \sqrt{\mathcal{E}_i'}\left(\frac{\Delta\mathcal{E}_i}{\mathcal{E}_i}\right)J_{i,s} \tag{A1}$$

to directly obtain partial-energy number densities for each ion species, s, over the spacecraft potential-adjusted energy range of HOPE $\left(\mathcal{E}_i' = \mathcal{E}_i + e\Phi_{SC}\right)$. Note that the term $\Delta\mathcal{E}_i/\mathcal{E}_i$ is not calculated in potential-adjusted (primed) energy coordinates, as it is a response function of the instrument. The HOPE omnidirectional flux data are used for this calculation, and isotropy is assumed. The reported energy resolution ($\Delta\mathcal{E}_i/\mathcal{E}_i$) is 16% at 1 eV and 12% at 50 keV [*Funsten et al.*, 2013]. The variation of $\Delta\mathcal{E}_i/\mathcal{E}_i$ over this range is given in the HOPE flux data files. *Goldstein et al.* [2014] used this method to calculate partial densities over the energy range 30 eV $\leq \mathcal{E} \leq$ 50 keV, compared the results with the densities calculated by the HOPE team (which excludes energies below ~30 eV), and found the two methods to produce nearly identical densities. The error in this method for calculating partial-energy number densities should scale with the (≥second-order) truncated terms in this first-order numerical integration scheme and with the Poisson uncertainty from the instrument count rate.

Appendix B: Error Analysis

Standard σ uncertainties can be obtained for the fit-determined temperature during the least squares fitting process. For the time interval examined in this study (see section 4), $2\sigma_T$ (95% confidence level) was generally low, with typical values being ~10% of the temperature (mean $2\sigma_T/T$ of 8%). We do not consider this method of uncertainty evaluation to be exceedingly useful, as $2\sigma_T/T$ is visibly and considerably smaller than additional sources of error, e.g., error that arises from the periodic differences in the HOPE and spacecraft spin phases (see oscillations in Figure 2f and the discussion in section 4.1). Additional errors should come from (1) overlap between the plasmasphere and ring current, (2) non-Maxwellian characteristics of the exceedingly cold portion of the plasmasphere, i.e., the portion of the distribution that is below the energy range of HOPE (note that errors from non-Maxwellian characteristics of the plasma within the energy range of HOPE should be accounted for by σ_T), and (3) differences between the model-determined bulk velocity and the actual bulk velocity of the plasmasphere. The phase space density data used in the fitting technique is weighted by Poisson error, so error source (1) should only be considerable when the relative densities of the two populations are comparable. When the densities are comparable, we expect that the fit method would overestimate the temperature and underestimate the density. Both (2) and (3) are either difficult or impossible to account for explicitly.

Using median values of the density (770 cm^{-3}, determined from EMFISIS and EFW), effective bulk velocity (5.61 km/s, determined from the modeled $\vec{E} \times \vec{B}$ drift speed and calculated spacecraft velocity), spacecraft potential (0.47 V, determined from EFW), and temperature (0.50 eV), we generated artificial Maxwellian distribution functions at the HOPE energy cadence over the range $\mathcal{E}_{HOPE,min} \leq \mathcal{E} \leq 30$ eV. Random Poisson noise was added to the flux values for each energy step using the standard Interactive Data Language (IDL) random number generator function. These artificial distribution functions were then fitted using the same technique that was outlined in the top of this section. This process was repeated 500 times, such that the difference between the fit-determined temperature and the predefined temperature of the artificial distribution functions could be compared for multiple random-noise cases. We found that the fit-determined temperature differed from the predefined temperature by 9.0% with a standard deviation of ±6.8%, which is similar to the mean value of σ_T discussed above (8%). This error in the temperatures determined from these artificial distribution functions changed by less than ±1% when the initial guess used in the fit technique was changed by ±50%, which is consistent with similar tests of fit-determined temperatures calculated from real HOPE data.

The average error in the fit-determined density was 23% ± 19% for artificial Maxwellian distributions defined by the median values of plasma, field, and spacecraft parameters listed above. This is similar to the standard error in the fit-determined density ($2\sigma_n/n$) for real HOPE data, which was 20%. This is far lower, however, than the mean difference between the fit-determined and EFW/EMFISIS densities, which was 80%. These very large differences between the real (EMFISIS/EFW) and fit-determined densities likely come from error sources (1)–(3). The fit-determined density is, at all times, greater than the partial-energy number density calculated by numerical integration of HOPE fluxes, which is expected.

Inaccuracies in the estimated plasma bulk kinetic energy, $\mathcal{E}_{bulk}\left(=\frac{1}{2}m\left|\vec{u}_{E\times B}-\vec{V}_{SC}\right|^2\right)$, are a source of error for both the fit-based and PEND methods. For the PEND method, it is relatively straightforward to derive an analytical relationship between an initial error in $\mathcal{E}_{bulk}$ and the resulting error in the temperature, T. We define $\mathcal{E}^{\star}_{bulk}$ to be an inaccurate value of the bulk kinetic energy $\left(\mathcal{E}^{\star}_{bulk}=\mathcal{E}_{bulk}\left[1+\epsilon_{\mathcal{E}}\right]\right)$ and $T^{\star}$ to be an inaccurate temperature, which is calculated from equation (5) with $\mathcal{E}^{\star}_{bulk}$, e.g., $T^{\star}=T\left(\mathcal{E}^{\star}_{bulk}\right)$. Using equation (5), the relative error in the temperature can be written as

$$\frac{T-T^{\star}}{T}=\frac{\mathcal{E}^{\star}_{bulk}/\mathcal{E}_{bulk}}{\mathcal{E}'_{HOPE,min}/\mathcal{E}_{bulk}-1}=\frac{\epsilon_{\mathcal{E}}}{\mathcal{E}'_{HOPE,min}/\mathcal{E}_{bulk}-1}, \tag{B1}$$

where $\mathcal{E}'_{HOPE,min}$ is the minimum particle energy that can be observed by HOPE, taken in this study to be $\mathcal{E}'_{HOPE,min}=\mathcal{E}_{HOPE,min}+e\Phi_{SC}\approx 1\ eV+e\Phi_{SC}$, where $\mathcal{E}_{HOPE,min}$ is the lowest energy channel of the instrument (1 eV for HOPE during its nominal survey mode) and Φ_{SC} is the spacecraft potential.

Equation (B1) shows that errors in the bulk kinetic energy should produce larger errors in the temperature if and when the bulk kinetic energy approaches the minimum energy that can be observed by the instrument (note that this was not observed in our case study, however). Because $\vec{V}_{SC}$ can be calculated directly from

ephemeris data, errors in $\mathcal{E}_{\text{bulk}}$ should come predominantly from the modeled magnetospheric electric field, $\vec{E}_M$, which is described in section 3.1 and used to calculate $\vec{u}_{E\times B}\left(=\vec{E}_M\times\vec{B}/B^2\right)$.

Equation (B1) can be expanded further to isolate this particular source of error. We define an absolute error in the magnetospheric electric field, $\vec{\delta}_E$, such that

$$\mathcal{E}^{\star}_{\text{bulk}}=\frac{m}{2}\left|\frac{\left(\vec{E}_M+\vec{\delta}_E\right)\times\vec{B}}{B^2}-\vec{V}_{\text{SC}}\right|^2, \tag{B2}$$

and

$$\epsilon_{\mathcal{E}}=\frac{1+\vec{\delta}_E\times\vec{B}/B^2\cdot\left[\vec{\delta}_E\times\vec{B}/B^2+2\vec{E}_M\times\vec{B}/B^2-2\vec{V}_{\text{SC}}\right]}{\left[\vec{E}_M\times\vec{B}/B^2-\vec{V}_{\text{SC}}\right]^2}. \tag{B3}$$

The largest values for $\epsilon_{\mathcal{E}}$ are obtained when $\vec{\delta}_E\times\vec{B}/B^2$ is aligned with the bulk velocity in the spacecraft frame, $\vec{E}_M\times\vec{B}/B^2-\vec{V}_{\text{SC}}$, so

$$\epsilon_{\mathcal{E}}\le\left[1+\left|\frac{\vec{\delta}_E\times\vec{B}/B^2}{\vec{E}_M\times\vec{B}/B^2-\vec{V}_{\text{SC}}}\right|\right]^2. \tag{B4}$$

This can be combined with equation (B1) to obtain an ultimate expression for the relative error in the temperature as a function of $\vec{\delta}_E$.

$$\frac{T-T^{\star}}{T}\le\frac{\left[1+\left|\frac{\vec{\delta}_E\times\vec{B}/B^2}{\vec{E}_M\times\vec{B}/B^2-\vec{V}_{\text{SC}}}\right|\right]^2}{\mathcal{E}'_{\text{HOPE,min}}/\mathcal{E}_{\text{bulk}}-1}. \tag{B5}$$

This shows that the error in the PEND method should be large when (a) the bulk kinetic and minimum observable energies are similar and/or when (b) the velocity of the spacecraft, $\vec{V}_{\text{SC}}$, is small. If either of these conditions are met, then errors in the bulk velocity will translate to large errors in the temperature.

Similarly, additional errors will arise if the temperature is calculated from an inaccurate measurement of the partial-energy number density, $n^{\star}_{\text{ESA}}=n_{\text{ESA}}(1+\epsilon_n)$, calculated from the electrostatic analyzer (ESA) data. The difference would most likely result from inexact calibration of the geometric factor at the instrument's lowest energy channels, as this calibration is difficult in either the laboratory or in space. The inaccurate temperature, $T^{\star}$, which is calculated from $n^{\star}_{\text{ESA}}$, can be expressed as

$$\frac{T-T^{\star}}{T}=\frac{\text{erf}^{-1}\left(1-\frac{n}{n_{\text{ESA}}}\right)-\text{erf}^{-1}\left(1-\frac{n}{n_{\text{ESA}}(1+\epsilon_n)}\right)}{\text{erf}^{-1}\left(1-\frac{n}{n_{\text{ESA}}}\right)}. \tag{B6}$$

This should only be a considerable error when the bulk kinetic and minimum observable energies are similar, as when this is the case, the partial-energy and total energy number densities should be comparable. For this case, we can approximate equation (B6) with the Taylor expansion of the inverse error function for $n_{\text{ESA}}\approx n$ as

$$\left[\frac{T-T^{\star}}{T}\right]_{n_{\text{ESA}}\to n}\approx\frac{\frac{1}{1+\epsilon_n}-1}{1-\frac{n_{\text{ESA}}}{n}}+\mathcal{O}\left(\left[1-\frac{n}{n_{\text{ESA}}}\right]^3\right). \tag{B7}$$

In equation (B7), we have only included the first term of the Taylor expansion, so the expression has a truncation error on the order of $\left(1-n/n_{\text{ESA}}\right)^3$.

Similar to equation (B5), equation (B7) shows that small errors in the input parameters (in this case, partial-energy number density) become a substantial source of error in the PEND method when the bulk kinetic and minimum observable energies become comparable. Conversely, the fit-based method for determining the temperature should be less error prone when $\mathcal{E}_{\text{bulk}}\to\mathcal{E}'_{\text{HOPE,min}}$, as only the width, rather than the amplitude, of the ESA-measured distribution function is required for this method.

In our case analysis of the plasmasphere intervals of 15 January 2013, we analyzed the differences in the temperature when large errors were purposefully introduced to the magnetospheric electric field and the ESA-measured partial-energy number density. When the magnitude of $\vec{E}_M$ was altered by ±100%, time-averaged differences of 3.3% and 1.2% were seen in the temperatures from the fit-based and PEND methods. These differences became much more significant at $L > 4$, where average differences of 17% and 3% were seen in the temperatures from the fit-based and PEND, respectively. When the ESA-measured partial-energy number densities were increased by 100%, the PEND temperature increased by 2.1%±1.7%. When the partial-energy number densities were decreased by 50%, the PEND temperature decreased by 1.9%±1.6%. The greater stability of the PEND technique as compared to the fit-based technique is to be expected for this event, as there were no instances where n_{HOPE} was larger than 1% of the total energy number density.

In the future, the full multidimensional space of the fit technique should be explored in order to better define its "working range." These dimensions include (1) total energy number density, (2) fractional total-to-partial-energy number density, (3) effective bulk velocity, (4) spacecraft potential, and (5) overlap between low- and high-energy plasmas. Additional work might be done in the future to determine "acceptable" levels of error in model-determined parameters, such as those that are used to determine the bulk kinetic energy.

Acknowledgments

Van Allen Probes HOPE data were obtained from the ECT team web page (http://www.rbsp-ect.lanl.gov). EFW data were obtained from the EFW team web page (http://www.space.umn.edu/rbspefw-data). The authors would like to thank those who contributed to the success of the Van Allen Probes mission. The work of Trinity University-affiliated coauthors was supported by the Zilker Endowment for Physics and Astronomy. Work at Los Alamos National Laboratory was performed under the auspices of the U.S. Department of Energy, approved for unlimited release: LA-UR-16-23592. The majority of this project was a result of volunteered time and independent research. Kevin Genestreti would like to thank the coauthors of this study and Lois Sarno-Smith for their time and enthusiasm, without which this study would not have been possible, and Jorg-Micha Jahn and Stephen Fuselier for their support and helpful suggestions.

References

Burch, J. L., J. Goldstein, and B. R. Sandel (2004), Cause of plasmasphere corotation lag, *Geophys. Res. Lett.*, *31*, L05802, doi:10.1029/2003GL019164.

Chappell, C. R., M. M. Huddleston, T. E. Moore, B. L. Giles, and D. C. Delcourt (2008), Observations of the warm plasma cloak and an explanation of its formation in the magnetosphere, *J. Geophys. Res.*, *113*, A09206, doi:10.1029/2007JA012945.

Comfort, R. H. (1986), Plasmasphere thermal structure as measured by ISEE-1 and DE-1, *Adv. Space Res.*, *6*(3), 31–40, doi:10.1016/0273-1177(86)90314-5.

Comfort, R. H. (1996), Thermal structure of the plasmasphere, *Adv. Space Res.*, *17*, 175–184, doi:10.1016/0273-1177(95)00710-V.

Comfort, R. H., J. H. Waite Jr., and C. R. Chappell (1985), Thermal ion temperatures from the retarding ion mass spectrometer on DE 1, *J. Geophys. Res.*, *90*, 3475–3486, doi:10.1029/JA090iA04p03475.

Comfort, R. H., I. T. Newberry, and C. R. Chappell (1988), Preliminary statistical survey of plasmaspheric ion properties from observations by De 1/RIMS, in *Modeling Magnetospheric Plasma*, pp. 107–114, AGU, Washington, D. C., doi:10.1029/GM044p0107.

Funsten, H. O., et al. (2013), Helium, Oxygen, Proton, and Electron (HOPE) mass spectrometer for the radiation belt storm probes mission, *Spa. Sci. Rev.*, *179*, 423–484, doi:10.1007/s11214-013-9968-7.

Fuselier, S. A., and B. J. Anderson (1996), Low-energy He^+ and H^+ distributions and proton cyclotron waves in the afternoon equatorial magnetosphere, *J. Geophys. Res.*, *101*, 13,255–13,266, doi:10.1029/96JA00292.

Gallagher, D. L., and R. H. Comfort (2016), Unsolved problems in plasmasphere refilling, *J. Geophys. Res. Space Physics*, *121*, 1447–1451, doi:10.1002/2015JA022279.

Goldstein, J., and B. R. Sandel (2005), The global pattern of evolution of plasmaspheric drainage plumes, in *Inner Magnetosphere Interactions: New Perspectives From Imaging*, vol. 159, p. 1, AGU, Washington, D. C.

Goldstein, J., B. R. Sandel, M. R. Hairston, and P. H. Reiff (2003), Control of plasmaspheric dynamics by both convection and sub-auroral polarization stream, *Geophys. Res. Lett.*, *30*, 2243, doi:10.1029/2003GL018390.

Goldstein, J., J. L. Burch, and B. R. Sandel (2005), Magnetospheric model of subauroral polarization stream, *J. Geophys. Res.*, *110*, A09222, doi:10.1029/2005JA011135.

Goldstein, J., S. D. Pascuale, C. Kletzing, W. Kurth, K. J. Genestreti, R. M. Skoug, B. A. Larsen, L. M. Kistler, C. Mouikis, and H. Spence (2014), Simulation of Van Allen Probes plasmapause encounters, *J. Geophys. Res. Space Physics*, *119*, 7464–7484, doi:10.1002/2014JA020252.

Gurgiolo, C., B. R. Sandel, J. D. Perez, D. G. Mitchell, C. J. Pollock, and B. A. Larsen (2005), Overlap of the plasmasphere and ring current: Relation to subauroral ionospheric heating, *J. Geophys. Res.*, *110*, A12217, doi:10.1029/2004JA010986.

Khazanov, G. V., T. E. Moore, E. N. Krivorutsky, J. L. Horwitz, and M. W. Liemohn (1996), Lower hybrid turbulence and ponderomotive force effects in space plasmas subjected to large-amplitude low-frequency waves,*Geophys. Res. Lett.*, *23*, 797–800, doi:10.1029/96GL00844.

Kotova, G., V. Bezrukikh, M. Verigin, and J. Smilauer (2008), New aspects in plasmaspheric ion temperature variations from INTERBALL 2 and MAGION 5 measurements, *J. Atmos. Sol. Terr. Phys.*, *70*, 399–406, doi:10.1016/j.jastp.2007.08.054.

Kotova, G. A. (2007), The Earth's plasmasphere: State of studies (a review), *Geomagn. Aeron.*, *47*, 409–422, doi:10.1134/S0016793207040019.

Lemaire, J. F., and K. I. Gringauz (1998), *The Earth's Plasmasphere*, p. 372, Springer, New York.

Mauk, B. H., N. J. Fox, S. G. Kanekal, R. L. Kessel, D. G. Sibeck, and A. Ukhorskiy (2013), Science objectives and rationale for the Radiation Belt Storm Probes mission, *Space Sci. Rev.*, *179*, 3–27, doi:10.1007/s11214-012-9908-y.

Sarno-Smith, L. K., M. W. Liemohn, R. M. Katus, R. M. Skoug, B. A. Larsen, M. F. Thomsen, J. R. Wygant, and M. B. Moldwin (2015), Postmidnight depletion of the high-energy tail of the quiet plasmasphere, *J. Geophys. Res. Space Physics*, *120*, 1646–1660, doi:10.1002/2014JA020682.

Sarno-Smith, L. K., B. A. Larsen, R. M. Skoug, M. W. Liemohn, A. Breneman, J. R. Wygant, and M. F. Thomsen (2016), Spacecraft surface charging within geosynchronous orbit observed by the Van Allen Probes, *Space Weather*, *14*, 151–164, doi:10.1002/2015SW001345.

Spence, H. E., et al. (2013), Science goals and overview of the Radiation Belt Storm Probes (RBSP) Energetic Particle, Composition, and Thermal Plasma (ECT) Suite on NASA's Van Allen Probes Mission, *Space Sci. Rev.*, *179*, 311–336, doi:10.1007/s11214-013-0007-5.

Stern, D. P. (1975), The motion of a proton in the equatorial magnetosphere, *J. Geophys. Res.*, *80*, 595–599, doi:10.1029/JA080i004p00595.

Volland, H. (1973), A semiempirical model of large-scale magnetospheric electric fields, *J. Geophys. Res.*, *78*, 171–180, doi:10.1029/JA078i001p00171.

Wygant, J. R., et al. (2013), The electric field and waves instruments on the Radiation Belt Storm Probes mission, *Space Sci. Rev.*, *179*, 183–220, doi:10.1007/s11214-013-0013-7.